Journal of Low Temperature Physics
https://doi.org/10.1007/s10909-020-02409-2

Demonstration of Fine-Pitch High-Resolution X-ray Transition-Edge Sensor Microcalorimeters Optimized for Energies below 1 keV

K. Sakai[1,2] · J. S. Adams[1,2] · S. R. Bandler[1] · S. Beaumont[1,2] · J. A. Chervenak[1] · A. M. Datesman[1,3] · F. M. Finkbeiner[1,4] · R. L. Kelley[1] · C. A. Kilbourne[1] · A. R. Miniussi[1,2] · F. S. Porter[1] · J. E. Sadleir[1] · S. J. Smith[1,2] · N. A. Wakeham[1,2] · E. J. Wassell[1,3] · F. T. Jaeckel[5] · D. McCammon[5] · M. E. Eckart[6] · K. Ryu[7]

Received: 20 August 2019 / Accepted: 10 February 2020

Abstract

In this paper, we report on X-ray transition-edge sensor (TES) microcalorimeters optimized to have the best possible energy resolution for a limited energy range for the incoming X-rays, such as an energy resolution of 0.3 eV full width half maximum (FWHM) for energies up to ≈ 0.8 keV as is desirable for one of the Lynx X-ray Microcalorimeter subarrays. The test array we have fabricated has 60×60 sensors on a pitch of 50 μm, and has 46×46 μm^2 absorbers that are one micrometer thick. We have measured a spectral energy resolution of the same device using 3 eV photons delivered through an optical fiber. For the one-photon 3 eV line, we have obtained an energy resolution of 0.25 eV FWHM, which is consistent with the estimated performance based on the signal size and noise. Further measurements will determine how the energy resolution degrades with energy. Based upon measurements of the TES transition characteristics, it appears that this level of energy resolution should be achievable up to 0.5 keV, and the performance will then gradually degrade to the measured energy resolution of around 2.3 eV at 1.5 keV. In this paper, we describe the full design and characterization of this detector, and discuss the performance limits of pixels designs like this.

Keywords Transition-edge sensors · Microcalorimeters · Lynx LXM

✉ K. Sakai
Kazuhiro.Sakai@nasa.gov

[1] NASA Goddard Space Flight Center, Greenbelt, MD 20771, USA

[2] CRESST II – University of Maryland, Baltimore County, MD 21250, USA

[3] KBRwyle, Lexington Park, MD 20653, USA

[4] Sigma Space Corp., 4600 Forbes Blvd., Lanham, MD 20706, USA

[5] University of Wisconsin-Madison, Madison, WI 53706, USA

[6] Lawrence Livermore National Laboratory, Livermore, CA 94550, USA

[7] MIT Lincoln Laboratory, Lexington, MA 02421, USA

Published online: 07 March 2020

1 Introduction

We are developing arrays of fine-pitch X-ray TES microcalorimeters for use in future space-based X-ray astrophysics missions such as the proposed Lynx X-ray Microcalorimeter. The Lynx mission is one of four flagship mission concepts currently being studied for consideration in the 2020 Astrophysics Decadal Survey [1]. The Lynx X-ray Microcalorimeter (LXM), one of three instruments the spacecraft carries, is a microcalorimeter detector consisting of one main array and two subarrays [2]. One of the subarrays is the "Ultra-high-resolution (UHR) array," which covers $1' \times 1'$ FOV with $1''$ pixels and provides 0.3 eV over the 0.2–0.75 keV energy band.

We have fabricated a test UHR array that has 60×60 TESs on a pitch of 50 μm. The TES is a 20 μm square superconducting Mo(40 nm)/Au(250 nm) bilayer, and each sensor has a $46 \times 46 \times 1\ \mu m^3$ gold absorber. The absorbers are cantilevered a few μm above the TES and supported by pillar-shaped stems at the center of each TES. For this array, the internal 64 pixels are wired using buried multilayer microstrip wires, wired with a density consistent with being able to wire out the complete array. The buried microstrip wires are underneath a planarized SiO_2 insulation layer. The wires make contact to the TES through two vias, as shown in Fig. 1a. The TES bilayer is then deposited on top of the leads and vias (Fig. 1b). Figure 1c shows the SEM image of the fabricated test array. Currently, the array is supported by a Si substrate in a geometry in which there is significant thermal cross-talk between nearby pixels [3]. Future generations of these arrays will eliminate this known source of energy resolution degradation by removing most of the silicon underneath the TESs, and integrating a high conductivity metallic layer to greatly reduce thermal cross-talk, as has been demonstrated previously [4].

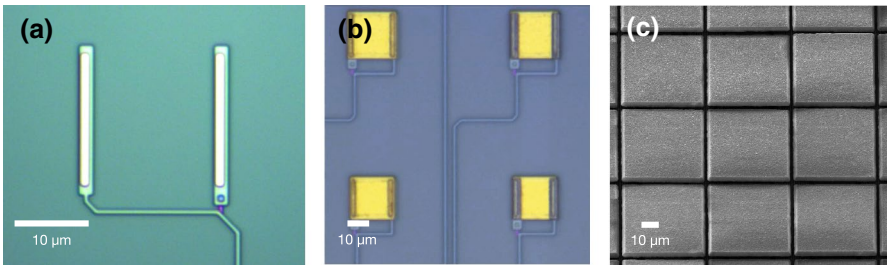

Fig. 1 (Color figure online) The buried microstrip wires underneath a SiO_2 planarized insulation layer and two vias **a** before the TES deposition and **b** after the TES deposition. **c** The SEM image of the fabricated array

2 Measurement Results

We first measured the fundamental characteristics of the TES. The experimental setup is described elsewhere [5]. From measurements of $I(V)$ at various bath temperatures, the TES Joule heating $P_0 = R_0 I_0^2$, where R_0 is the TES resistance and I_0 is the TES current, was calculated for each bath temperature. These data were fit to the formula $P_0 = K(T_0^n - T_{\rm bath}^n)$, where K and n are thermal link constants, T_0 is the TES temperature, and $T_{\rm bath}$ is the bath temperature. Using K, n, and T_0, the thermal conductance from TES to the bath, $G_{\rm b}$, was then calculated. This calculation assumes that T_0 is a constant value for all $T_{\rm bath}$ if biased at the same R_0. However, this is only valid when the TES resistance is not strongly current dependent. The small TES in this study has a strong current-dependent transition, and therefore, P_0 was obtained from the top of the transition where the current dependence becomes negligible [6].

We have measured those characteristics individually for some pixels, and for one pixel at the center of the array we have obtained $G_{\rm b} = 151\,{\rm pW/K}$ at 100 mK. Other pixels also showed very similar results, and hereafter all the results in this paper are for that pixel as a representative of the array. With $G_{\rm b}$, $R(T)$ was calculated for $T_{\rm bath} = 42\,{\rm mK}$, which is shown in Fig. 2. $\alpha_{IV} = d\log R/d\log T$ was then calculated from $R(T)$, which is also shown in Fig. 2. The transition is very smooth from the superconducting state to the normal state. For the spectral measurements described below, we bias the TES at 2.5% of the normal resistance (16 mΩ), in a bias circuit that has a parallel shunt resistance of 0.2 mΩ.

An X-ray source within the desired range of X-ray energies for this device, with known intrinsic linewidth and sufficient flux, was not available. Using a commercial X-ray source[1] with an Al target, we measured the detector response to 1.5 keV X-rays, which is factor of two higher than the maximum X-ray energy targeted. The heat capacity of the pixel is optimized for X-rays less than 0.75 keV, and therefore the performance is expected to deteriorate at these energies due to the nonlinearity of the detector response. Figure 3 (left) shows the AlKα X-ray spectrum. The energy resolution (the broadening of the intrinsic linewidth of the Al source) is 2.3 ± 0.1 eV full width half maximum (FWHM) at 1.5 keV. The inset shows a gain calibration using a second-order polynomial based upon the measured AlKα and SiKα line energies, demonstrating that the microcalorimeter response is highly nonlinear.

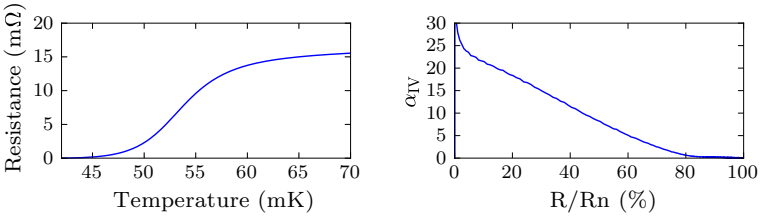

Fig. 2 (Color figure online) (Left) The TES transition curve for $T_{\rm bath} = 42\,{\rm mK}$. (Right) The calculated $\alpha_{\rm IV}$ curve from the transition curve

[1] Manson model 2 mini-focus ultrasoft X-ray source made by Austin Instruments, Inc.

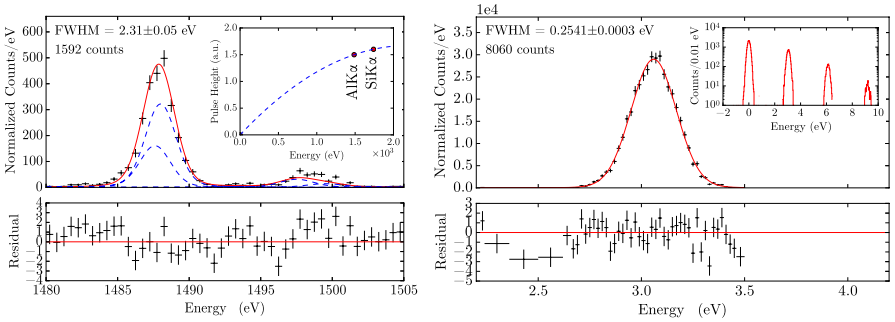

Fig. 3 (Color figure online) (Left) Measured Al-Kα energy histogram. The blue-dashed lines show the known fine-structure lines convolved with the detector response assuming a FWHM of 2.3 eV. The solid red line shows the best fit to the data assuming a FWHM energy resolution of the detector of 2.31 eV. The residuals for the fit are shown below. *Inset*: Gain calibration based upon AlKα and SiKα lines. (Right) The 3-eV spectrum with the best-fitted line model. The energy resolution is 0.25 eV FWHM. *Inset*: The full range spectrum in a log scale

For low-energy calibration, we have used an optical "Blu-Ray" laser diode, which has a linewidth of 1 nm around 405 nm, and delivered 3.06 eV photons through an optical fiber to the detector. This method is described elsewhere [7]. The diode is at 300 K outside the dewar, and excited by 1 µs electrical pulses to generate photons. Due to low optical throughput arising from the difficulty of aligning a 25 µm aperture over the pixel, we were only able to observe 3, 6, 9, and 12 eV combs in spectra, corresponding to one, two, three, and four photons being absorbed by the pixel during a single excitation pulse. Figure 3 shows the spectrum for 3.06 eV photons as well as the best-fitted model. The energy resolution is 0.2541 ± 0.0003 eV FWHM, which is within the LXM requirement. Although the statistics are low, we have also obtained an energy resolution of 0.256 ± 0.001 eV FWHM for the 6 eV two-photon peak.

3 Analysis

To help determine the energy resolution performance between 6 eV and 1.5 keV, we have estimated the predicted energy resolution based upon the heat capacity and measurable transition parameters. The heat capacity of the device, C_{TES}, was derived from the decay time of 1.5 keV X-rays pulses when biased high in the transition where the electrothermal feedback is negligible. We have measured the decay time at various bath temperatures from 80 to 190 mK and derived the heat capacity. Figure 4 shows this measured heat capacity as a function of bath temperature. The dashed line in the same figure is the expected heat capacity calculated from the geometry of the absorber assuming it is all gold. The measured heat capacity shows an offset of ~ 15 fJ/K. Such an offset is not typical for a metallic absorber and is likely due to a fabrication contamination in this particular array.

The transition parameters, $\alpha = \partial \log R / \partial \log T$ and $\beta = \partial \log R / \partial \log I$, were obtained from measurements of the complex impedance (Z) of the device at various

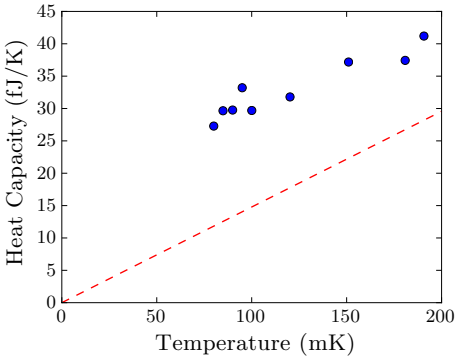

Fig. 4 (Color figure online) The derived device heat capacity as a function of the bath temperature. The dashed line is the expected heat capacity calculated from the geometry of the absorber assuming it is all gold

bias points and frequencies, and then from fitting Z to a single-body model in which the pixel is assumed to be a simple single heat capacity [8]. From this measured α and β, together with the other measured TES characteristics, we reconstructed an X-ray pulse at various bias points by solving the standard nonlinear electrical and thermal differential equations [9]. The predicted energy resolution in the small-signal limit for each bias point was then calculated using the reconstructed pulse and the noise from the measurement. Figure 5 shows α, β, the TES temperature, and the predicted energy resolution for various bias points up to 40% of R_0/R_n, where R_n is the normal-state resistance.

From the measured heat capacity, the temperature increase in the device for 0.75 keV X-ray is calculated as ~ 5 mK when the device is biased at 2.5% of R_0/R_n.

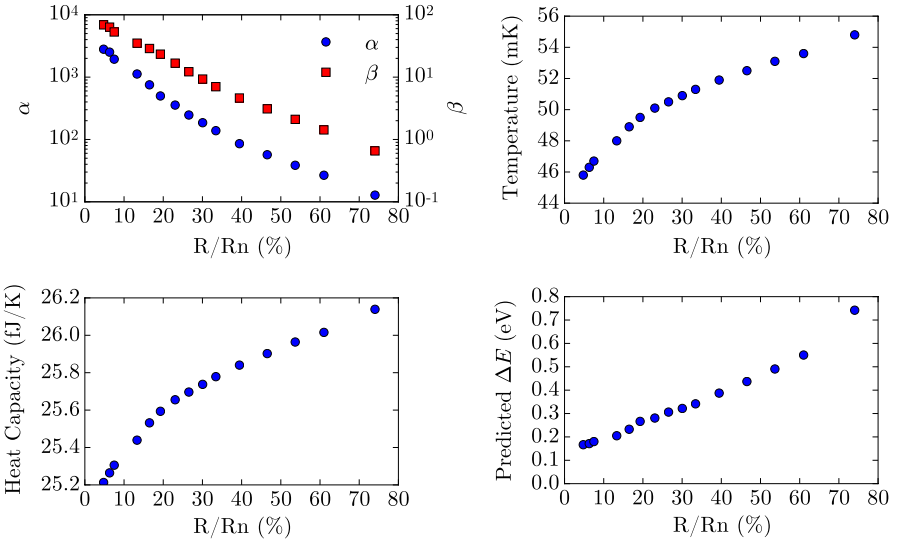

Fig. 5 (Color figure online) (Top Left) α and β obtained from the complex impedance measurement at $T_{bath} = 42$ mK. (Top Right) The TES temperature calculated from I_0, R_0, K, n, and T_{bath}. (Bottom Left) The TES heat capacity. (Bottom Right) The predicted energy resolution in the small-signal limit

The temperature excursion of the device therefore is from 46 to 51 mK, which is roughly equivalent to a 30% of R_0/R_n where the predicted energy resolution is ~ 0.3 eV FWHM. Therefore, a rough estimate for the achievable energy resolution for 0.75 keV is 0.3 eV FWHM, which would meet the Lynx requirement; however, further measurements at energies up to 0.75 keV are needed to verify this.

4 Summary

We have fabricated a test array of prototype "Ultra-high-resolution array" pixels for the Lynx X-ray Microcalorimeter, with pixels on a 50 µm pitch using a 20 µm TES and $46 \times 46 \times 1$ µm^3 Au absorbers. The TES bias wires were buried beneath the surface of the array substrate, with an insulation layer above, and connected to the TES through two vias close to the TES. This device was optimized for energies below 0.75 keV. We have measured 2.31 eV FWHM at 1.49 keV and 0.25 eV FWHM at 3 eV. We have estimated the energy resolution using α, β, C_{TES}, and the measured noise. For 0.75 keV, which is the upper limit of the Lynx requirement on the energy band, we estimate that the energy resolution performance could be as good as 0.3 eV FWHM, which would meet the Lynx requirement.

Acknowledgements Part of this work was performed under the auspices of the U.S. Department of Energy by Lawrence Livermore National Laboratory under Contract DE-AC52-07NA27344. The MIT Lincoln Laboratory portion of the work is based upon work supported by the United States Air Force under Air Force Contract No. FA8702-15-D-0001. Any opinions, findings, conclusions or recommendations expressed in this material are those of the author(s) and do not necessarily reflect the views of the United States Air Force.

References

1. J.A. Gaskin et al., JATIS **5**, 2 (2019). https://doi.org/10.1117/1.JATIS.5.2.021001
2. S.R. Bandler et al., JATIS **5**, 2 (2019). https://doi.org/10.1117/1.JATIS.5.2.021017
3. N. Iyomoto et al., IEEE Trans. Appl. Supercon. **19**, 557 (2009). https://doi.org/10.1109/TASC.2009.2017704
4. F.M. Finkbeiner et al., IEEE Trans. Appl. Supercon. **21**, 223 (2011). https://doi.org/10.1109/TASC.2010.2091237
5. S.J. Smith et al., J. Appl. Phys. **114**, 7 (2013). https://doi.org/10.1063/1.4818917
6. C.N. Bailey et al., J. Low Temp. Phys. **167**, 121 (2012). https://doi.org/10.1007/s10909-012-0562-2
7. F.T. Jaeckel et al., IEEE Trans. Appl. Supercon. (2019). https://doi.org/10.1109/TASC.2019.2899856
8. N. Iyomoto et al., Appl. Phys. Lett. **92**, 013508 (2008). https://doi.org/10.1063/1.2830665
9. K.D. Irwin, G.C. Hilton, *Cryogenic Particle Detection*, vol. 99 (Springer, Berlin, 2005)